Functional morphology of vertebrate feeding systems: new insights from XROMM and fluoromicrometry

Elizabeth L. Brainerd and Ariel L. Camp

Abstract Investigations into the form-function relationships of vertebrate feeding systems have a long and illustrious history of inferring function from anatomical structure and specimen manipulation, and a shorter but highly successful history of measuring function directly in living animals with sophisticated methods such as electromyography, bone strain gauges, high-speed cinematography and cineradiography. Two new methods, X-ray Reconstruction of Moving Morphology (XROMM) and fluoromicrometry show great promise for revealing the 3D form-function relationships of cranial and cervical musculoskeletal structures. XROMM has been applied to measure 3D jaw kinematics and tooth occlusion in mammalian mastication and 3D pharyngeal jaw mechanics in fishes. The form-function relationships of the temporomandibular and other cranial joints are being explored with XROMM, including cranial kinesis in squamates, birds and fishes. Muscle strain can be measured with fluoromicrometry by implanting small radio-opaque beads and tracking them with biplanar fluoroscopy. Fluoromicrometry has been used to measure muscle strain in muscles with complex architectures, such as the axial muscles during suction feeding in fishes and tongue deformation during swallowing in mammals. XROMM combined with fluoromicrometry and buccal pressure measurements have been used to measure the instantaneous power required for suction feeding and relate required power to available muscle power. In the future, some systems that may benefit greatly from XROMM and fluoromicrometry are tooth-food interactions during mastication, food transport and swallowing, and the form-function relationships of feeding muscles with complex muscle-tendon architecture, such as the mammalian muscles of mastication and the multi-part adductor mandibulae of fishes.

E.L. Brainerd (elizabeth_brainerd@brown.edu)
Department of Ecology and Evolutionary Biology
Brown University
Providence RI 02912
USA

A.L. Camp (Ariel.Camp@liverpool.ac.uk)
Department of Musculoskeletal Biology
Institute of Ageing and Chronic Disease
University of Liverpool
Liverpool L7 8TX
UK

2.1 Introduction

Some of the form-function relationships between head structures and feeding performance are fairly obvious and quite satisfying. Teeth in particular are often unmistakably the right tools for the job at hand: herbivorous vertebrates tend to have flat, ridged teeth for grinding plant matter, carnivores have knife-like blades for slicing flesh and durophagous vertebrates have flat teeth for breaking prey without breaking their teeth. Teeth are a prominent component of the vertebrate fossil record, extending these form-function inferences into the deep past. Analogies with human tools also suggest inferences about jaw shape and biting, with short jaws being analogous to pliers generating high bite forces and long jaws analogous to hedge trimming shears with rapid closure at the tips.

The mechanical functions of feeding systems, such as those mentioned above, traditionally were inferred from morphology and manipulation of dead specimens, but extensive work to measure function directly in live animals began in the middle of the 20th century and grew rapidly. Electromyography (EMG), high-speed cinematography and cineradiography were applied to both aquatic and terrestrial feeding systems, and particularly to suction feeding in ray-finned fishes (e.g. (Anker 1974; Grobecker and Pietsch 1979; Osse 1969)) and mastication in mammals (e.g. (Ardran et al. 1958; Becht 1953; Moyers 1950); reviewed in (Gans et al. 1978)). High-speed film was replaced with high-speed video in the late 1980s and then digital high-speed video in the 1990s, greatly speeding up the pace of research on animal motion (Lauder and Madden 2008). In the late 1970s, researchers began surgical implantation of strain gauges, adhering them to the bone surface to measure mandibular strain during mastication in mammals (e.g. (Hylander 1977; Weijs and De Jongh 1977)). Sonomicrometry has been applied extensively to measure muscle strain, i.e., the change in a muscle's length relative to its initial length, during locomotion, and has seen some use in feeding systems for measuring muscle strain (e.g. (Carroll 2004; Konow et al. 2010)) and other distances through liquids or soft tissues (Sanford and Wainwright 2002). In sonomicrometry, two or more piezoelectric crystals are implanted within the muscle, and can send and receive electrical pulses. The distance between two crystals, and thus the length of the muscle, can be calculated based on the time required for a pulse to travel between the crystals and the speed of sound in an aqueous medium. In the early 2000s,

transducers for measuring bite force gained prominence and have been used in studies of many terrestrial and aquatic vertebrates (e.g. (Herrel et al. 2001) and reviewed in (Anderson et al. 2008)).

In addition to all of these methods for measuring feeding behavior in vivo, methods for 3-dimensional (3D) quantification of morphology ex vivo have developed rapidly and gained widespread use in the past two decades. X-ray computed tomography (CT) scanning was adapted for 3D skeletal morphology in extant vertebrates and fossils in the 1980s and 1990s (e.g. (Conroy and Vannier 1984; Cranford 1988; Rowe et al. 1999; Rowe et al. 1995)), and later methods were developed for staining soft tissues to create X-ray contrast for CT (Gignac and Kley 2014; Jeffery et al. 2011; Metscher 2009). Microsource CT (microCT) produces high resolution scans of small animals, and recent efforts to standardize CT data management and open data practices promise to vastly increase the value of CT data for comparative studies (Davies et al. 2017). Other biomedical imaging modalities, such as Magnetic Resonance Imaging (MRI) and Positron Emission Tomography (PET), have found some use in comparative morphology (e.g. (Berquist et al. 2012; Gold et al. 2016; Montie et al. 2007)). The advent of contrast-enhanced CT has made the use of MRI for static soft tissue imaging less attractive, but MRI and PET offer some exciting possibilities for functional imaging (Gold et al. 2016; MacCannell et al. 2017; Phelps 2000).

The availability of 3D musculoskeletal morphology has led to great advances in 3D modeling of form-function relationships in feeding systems, particularly through finite element analysis (FEA) models of skeletal strain (reviewed in (Grosse et al. 2007; Rayfield 2007)), multi-body dynamics analysis (MDA) models of bite force (e.g. (Gröning et al. 2013; Watson et al. 2014)) and computational fluid dynamics models of suction feeding in fishes (e.g. (Van Wassenbergh and Aerts 2009)). A review of these modeling methods is beyond the scope of this chapter, but they are providing fundamental new insights into the functional morphology of feeding systems. They also show great promise for expanding the reach of functional morphology beyond in vivo measurements, such as to large datasets containing many species, to extinct vertebrates, and to in silico exploration of morphologies that may or may not actually occur in nature.

For studies of feeding in vivo, two new methods have been developed in recent years: X-ray Reconstruction of Moving Morphology (XROMM) and fluoromicrometry (Brainerd et al. 2010; Camp et al. 2016; Knörlein et al. 2016). Below we review and discuss the applications of these new methods to feeding systems, and consider some research questions that may particularly benefit from study with XROMM and fluoromicrometry.

2.2 Applications of X-ray Reconstruction of Moving Morphology (XROMM) to feeding systems

Much of what happens inside the oropharyngeal cavities during feeding is hidden by cheeks and other tissues. Cineradiography has revealed some of the actions of fleshy tongues, pharyngeal jaws, and teeth in the oral and pharyngeal regions, but cineradiography has historically provided only 2D views of complex 3D motions. A relatively new method, XROMM, is showing great promise for form-function studies of feeding because it yields simultaneous data on 3D skeletal kinematics and 3D bone shape. The 3D bone morphology usually comes from a CT scan, and 3D motion from biplanar videofluoroscopy. Polygonal mesh bone models from an individual animal are animated with motion from videofluoroscopy to match precisely, typically within 0.1 mm, the in vivo motions of the animal (Brainerd et al. 2010; Gatesy et al. 2010). The exact precision of an XROMM animation depends on multiple factors including the imaging volume, marker placement and tracking, and CT reconstruction (Knörlein et al., 2016), and is often better than 0.1 mm (e.g., Camp and Brainerd, 2015; Dawson et al., 2011; Gidmark et al., 2012; Konow et al., 2015).

The 3D kinematics of jaws is an excellent subject for XROMM analysis. Many studies are ongoing, but to date only a few have been published. In juvenile miniature pigs feeding on pig chow, XROMM demonstrated that the lower jaw yaws about a dorsoventral axis (Fig. 2.1) to produce the observed alternating left-right chewing cycles responsible for food reduction (Menegaz et al. 2015). This yaw of the entire lower jaw is produced by asymmetrical protrusion at the left and right temporomandibular joints (TMJs). By contrast, in ferrets and kinkajous, lateral motions of the mandible are produced by lateral translation of the mandibular condyles relative to the mandibular fossae, not yaw of the entire jaw (Davis 2014). In three species of non-

human primates, helical axis analysis of jaw depression and elevation showed that the axis of rotation of the mandible is located inferior to the TMJ, and this location varies among species (Iriarte-Diaz et al. 2017). In fishes, the pharyngeal jaws of grass carp were shown to grind grasses with an oblique grinding stroke shaped by the upper occlusion surface, a keratinous chewing pad (Gidmark et al. 2014). These studies demonstrate the ability of XROMM not only to reveal motions previously hidden by cheeks and other tissues, but also to quantitatively describe that motion using anatomically-relevant axes.

Temporomandibular joint shape varies substantially among mammals, and XROMM has the potential to reveal TMJ form-function relationships that could then be used to infer mandibular motion across many extant and extinct species. Thus far, the expected broad patterns have held: omnivorous pigs and primates have a broad, flat TMJs and show substantial bilateral and unilateral protrusion at the TMJ (Iriarte-Diaz et al. 2017; Menegaz et al. 2015), whereas carnivores, such as ferrets, have cylindrical TMJs that restrict motion to depression, elevation and lateral translation (Davis 2014). The functional significance, if any, of smaller differences in TMJ morphology among more closely related species remain to be explored with XROMM.

The broader form-function relationships of cranial joints are also being studied with XROMM (Olsen et al. 2017). In this approach, using channel catfish as a beginning model system, joint fitting routines extract the joint type, such as ball and socket, saddle or hinge, from large XROMM motion datasets of diverse motions from individual animals. Sets of joints in kinetic skulls, such as those of birds and fishes, can then be linked into 3D mechanisms that further determine the degrees of freedom of the system (Olsen and Westneat 2016). This approach has the potential to provide new insights into the form-function relationships of bones, joints, and linkage mechanisms, that could then be applied to large-scale studies of museum specimens of extant and extinct vertebrates.

The nature of tooth occlusion in mammals is particularly hard to study with traditional methods because, necessarily, during occlusion the chewing surfaces are visually occluded preventing any standard video analysis. The power of XROMM for studying tooth occlusion is that the mesh model from the CT scan includes all the detail of tooth morphology. The XROMM

animation then includes the position of every location on every tooth at all times. For example, in miniature pigs feeding on pig chow, XROMM demonstrated that the yaw of the mandible produces a grinding motion between upper and lower premolars that includes a substantial mesiodistal component, in addition to the expected buccolingual component, resulting in an oblique power stroke (Fig. 2.2). The evolutionary origin of jaw yaw as it relates to tooth occlusion and the muscles of mastication has recently been explored (Grossnickle 2017). These results from miniature pigs demonstrate that XROMM can be used to study the details of tooth-tooth interaction during tooth occlusion in mammals, a potentially fruitful direction for continuing to explore the form-function relationships of teeth.

Another finding from work on miniature pigs is that XROMM can reveal some information about the breakdown of the food bolus (Menegaz et al. 2015). Jaw kinematics from processing a Brazil nut in the shell showed evidence of when the nut broke and then gradual decrease in the distance between upper and lower teeth, as indicated by increasing jaw elevation (Fig. 2.3), as the size of the nut and shell fragments were reduced. These findings drive home the point that teeth in living animals work with food between them, not with the teeth occluding directly. Depending on the nature of the food, the form-function relationships of the teeth may be changing constantly during a bout of mastication as the particle size, consistency and bolus size change. With XROMM these tooth-food interactions can be studied directly, although work is needed to develop methods for radio-opaque marking of the food that will not obscure the teeth and may provide discrete information about food breakdown.

Unlike mammals, most vertebrates have many mobile skeletal elements within the skull and substantial intracranial kinesis. However, these motions are often three-dimensionally complex, involve structures not visible externally, or both, making them difficult to study in vivo with traditional video analysis. In squamates, mesokinesis has long been postulated from morphology and manipulation of dead specimens and has recently been confirmed in living Tokay geckos with XROMM (Montuelle and Williams 2015). In Tokay geckos, the snout rotates dorsally relative to the braincase during wide gape display behaviors and ventrally during defensive and feeding bites. In birds, the quadrate bone is the central junction of kinesis, suspending the lower bill and articulating via the palatal bridge to the upper bill. In ducks, an XROMM study showed

that 3D motions of the quadrate include mediolateral motions associated with lateral spreading of the hemimandibles and rostrocaudal motions associated with upper bill elevation and depression (Dawson et al. 2011). Ray-finned fishes are the champions of cranial kinesis with more than 20 mobile cranial and hyoid bones that contribute to food acquisition, transport and processing (Liem 1980). These cranial elements are linked in mechanisms, such as the opercular linkage, which is thought to contribute to lower jaw depression. Planar 4-bar linkage models have been shown to fit this mechanism poorly (Van Wassenbergh et al. 2005b; Westneat 1990; Westneat 1994), with XROMM demonstrating up to 50% over-estimate of lower jaw depression from opercular rotation in largemouth bass (Camp and Brainerd 2015). Working from 3D XROMM data, the best-fit model for the opercular mechanism was found to be a 3D, 3-DoF 4-bar linkage, achieving rotational errors of less than 5% (Olsen et al. 2017).

In studies of suction feeding in fishes, a longstanding problem has been our inability to make empirical measurements of the rate of expansion of the oropharyngeal cavity during this rapid behavior. Excellent work has been done modeling this expansion as an increasingly complex set of expanding cones or elliptical slices for fluid dynamic and computational fluid dynamic models of suction feeding (e.g. (Muller and Osse 1984; Muller et al. 1982; Van Wassenbergh and Aerts 2009; Van Wassenbergh et al. 2005a)) (Fig. 2.4). Now we can also measure rate of volume expansion directly with XROMM, by marking most of the cranial bones with tiny (0.5-0.8 mm) radio-opaque spheres, tracking them with biplanar videofluoroscopy and animating them with XROMM. These bones then define the outer shell of the oropharyngeal cavity, and a deformable polygon can be fit within the space to yield a dynamic digital endocast of the instantaneous volume at each time step (Fig. 2.5). The soft tissues within the mouth are not included, so the absolute volume of the endocast will always be a larger than the true volume, but the change in volume per time will be correct. Combined with pressure measured in the buccal cavity, the instantaneous suction power can be calculated throughout the suction feeding strike (Camp et al. 2015).

In some circumstances, XROMM can also be used to measure in vivo changes in muscle length. In muscles with fairly straight fascicles, simple architecture and no tendon, the attachment points of the muscle fascicles can be mapped onto the mesh models of the bones, the

bones animated with XROMM, and then the lengths of the fascicles measured at each time step (Fig. 2.6). This technique was used for the pharyngeal jaw levator muscle of the black carp, a durophagous cyprinid specializing on snails and other hard-shelled prey (Gidmark et al. 2013). The in vivo muscle lengths from XROMM were combined with *in situ* length-tension curves and in vivo shell-crushing performance to show that pharyngeal bite force drops off at both small and large pharyngeal jaw gapes resulting from small and large prey shell sizes. In this study, muscle strain in vivo could be measured from XROMM due to the levator muscle being a simple, fan-shaped muscle with no tendon (Fig. 2.6). The lack of fixed-end compliance, as would be found with a tendon or other series elasticity in the muscle, was confirmed with the in situ force-length recordings (Gidmark et al. 2013). Muscle strain was also measured from XROMM animations for some of the muscles of the head in largemouth bass (Camp et al., 2015) and bluegill sunfish (Camp et al., 2018): the levator operculi, dilator operculi, sternohyoideus and levator arcus palatini. These muscles also have fairly simple architecture and little or no tendon, and in one muscle, length measurements were also confirmed with radio-opaque beads implanted into the muscle belly (i.e., fluoromicrometry) (Camp et al. 2015).

However, when a free tendon or other source of fixed-end compliance is present, XROMM provides only the distance between attachment points on the bones, which is the length of the whole muscle-tendon unit (MTU) and not the length of the muscle fascicles. In these cases, muscle length changes should be measured directly with fluoromicrometry: implanting radio-opaque beads into the muscle belly, recording marker motion in vivo with biplane fluoroscopy, and tracking markers in 3D to measure muscle length changes from the intermarker distance changes. Fluoromicrometry, can yield muscle length measurements with a precision of 100 microns (Camp et al. 2016), although as with XROMM the precision may vary with the imaging setup and marker placement and tracking (Knörlein et al., 2016). Fluoromicrometry can be combined with XROMM to measure both muscle and tendon length by determining MTU length from XROMM and then subtracting muscle fascicle length changes from MTU length to get tendon length. In theory, fluoromicrometry could be used to measure tendon strain directly, but radio-opaque beads tend to get squeezed out of tendons when simply injected into the tissue (Camp et al. 2016), although beads sutured to an aponeurosis can yield aponeurosis strain (Azizi and Roberts 2009). The combination of fluoromicrometry and XROMM to measure MTU

length, muscle strain and tendon strain has been applied to jumping frogs and flying bats (Astley and Roberts 2012; Konow et al. 2015), but not yet to feeding systems.

2.3 Applications of Fluoromicrometry to Feeding Systems

Fluoromicrometry has been used to measure axial muscle strain during suction feeding in fishes and tongue deformation during swallowing in rhesus macaques (Camp and Brainerd 2014; Camp et al. 2015; Camp et al. 2017; Camp et al., 2018; Orsbon et al. 2017). As described above, the length changes in some cranial muscles of fishes can be measured directly from their attachment sites and the XROMM animations of cranial bones (Camp et al. 2015). The epaxial and hypaxial muscles of fishes, however, do not have discrete bony attachment sites. Instead, multiple tantalum beads (0.5-0.8 mm diameter) can be injected into the musculature to measure axial muscle strains throughout the epaxial and hypaxial muscle masses (Fig. 2.7). For studies such as this requiring many markers, fluoromicrometry offers an advantage over sonomicrometry, which can only simultaneously measure a limited number of pairwise distances and the maximum available sampling rate goes down with more crystals. The additional advantages of fluoromicrometry for measuring axial muscle strain are that radio-opaque tantalum beads can be placed by percutaneous injection with a hypodermic needle, no wires emerge from the animal and many pairwise distances can be measured simultaneously (Camp et al. 2016). Tantalum beads can also be injected medially, close to the axial skeleton to define a body-reference plane that can be used to measure cranial movements relative to the body (Fig. 2.7a).

In mammalian mastication, the rapid, 3D motions of the tongue and cheeks are extremely difficult to see and track, yet these motions are critical for bolus formation, bolus management and swallowing. Fluoromicrometry combined with XROMM and contrast-enhanced CT (DiceCT; (Gignac et al. 2016)) is starting to be applied to measure hyoid and jaw kinematics, hydrostatic tongue deformation, and muscle length changes (Orsbon et al. 2017; Orsbon et al. 2018). This work on complex jaw, hyoid and tongue motions emphasizes a great advantage of fluoromicrometry over sonomicrometry. Sonomicrometry yields only 2D distances, or at best a set of 3D distances relative to each other, but with no other anatomical context. Fluoromicrometry combined with XROMM yields both 3D bone kinematics and 3D soft tissue

marker motions simultaneously, providing actual 3D soft tissue deformations with reference to bone positions. Such data will be essential for discovering the remarkable neuromotor coordination of tongue, jaws and cheeks that allow mammals to chew and swallow so precisely and prevent tongue and cheek biting (usually) and choking (Orsbon et al. 2017; Orsbon et al. 2018).

2.4 XROMM and Fluoromicrometry Case Study: Measuring Suction Feeding Power in Fishes

Suction feeding in fishes is an amazing behavior because it is lightning fast and, to the naked eye, prey seem to just disappear into the predator's maw. Suction is produced by expansion of the entire oropharyngeal cavity (buccal and opercular cavities), sucking water and prey in through the mouth aperture. The water then flows out the gill openings, and the captured prey is retained in the pharynx and then swallowed. Accelerating a mass of water into the mouth requires substantial force, so suction feeding is both fast and forceful and therefore requires considerable muscle power (Carroll and Wainwright 2006; Van Wassenbergh et al. 2005a). Where does all that muscle power come from?

One might expect feeding to be powered by cranial muscles, but in most fishes these muscles are relatively small and may be insufficient to supply the power required for suction feeding (Fig. 2.8). We have known for a long time that epaxial muscles immediately behind the head contribute some power (e.g. (Liem 1967; Osse 1969)). Axial muscles are large in relation to cranial muscles, and evidence from empirical studies and modeling indicates that axial muscles must be contributing substantial power in many suction-feeding fishes (Carroll and Wainwright 2006; Gibb and Ferry-Graham 2005; Oufiero et al. 2012; Van Wassenbergh et al. 2008). But how much of the axial muscles (which extend from head to tail) contribute to feeding, and what proportion of suction expansion power do they generate?

Answering these questions requires simultaneous measurements of axial and cranial muscle shortening and instantaneous suction expansion power (Fig. 2.9). As described above, XROMM and the dynamic endocast method can be used to measure instantaneous buccal expansion rate

(Fig. 2.5). Instantaneous buccal pressure can be measured with a miniature pressure transducer, and pressure times rate of volume change yields instantaneous suction power (Fig. 2.9a). Fluoromicrometry can be used to measure axial muscle shortening and the extent of shortening along the body (Fig. 2.9b). The extent of shortening is needed to determine the mass of axial musculature that contributes to suction feeding, as only actively shortening muscles can generate power. Cranial muscle shortening can be determined from fluoromicrometry or muscle fascicle attachment points mapped onto the animated cranial bones (Fig. 2.9c). The maximum amount of power that could be generated by the cranial and axial muscles can be estimated from their masses, assuming optimal activation and shortening rate, yielding optimal muscle power capacity (P_{opt}). Actual muscle shortening rates from XROMM and fluoromicrometry (Fig. 2.10) can then be taken into account to estimate velocity-corrected power capacity (P_{vc}), which is a best estimate of the actual maximum power available from each muscle during any given strike (Fig. 2.9c).

Using these methods, we compared suction power to muscle power capacity and showed that at least 95% of the power for high-performance strikes comes from axial muscles in largemouth bass (Figs. 2.11 and 2.12). The epaxials and hypaxials have by far the largest P_{opt}, due to the large mass of muscle employed, and they also shorten consistently during peak power production (Fig. 2.10). In contrast, the P_{opt} of the cranial muscles can hardly be seen on the same scale as the axial muscles (Fig. 2.12). Only the sternohyoideus shows substantial potential for power generation, P_{opt}, but in fact on average it does not shorten during peak power production (Fig. 2.10), and hence realizes near zero P_{vc} (Fig. 2.12). These results indicate that largemouth bass use the bulk of their axial muscles for high power strikes, transferring power from the axial to the cranial systems. This power transfer is analogous to athletic feats in many human sports: just as baseball pitchers transfer power efficiently from their legs and core to their throwing arms, so largemouth bass transfer power from body to head.

Our finding that most of the axial muscle mass is recruited for suction feeding suggests that we may need to reconsider the structure and function of these body muscles in fishes. While the red musculature along the lateral sides of the body and the musculature near the tail may function for swimming only, the bulk of the white axial musculature likely has dual functions in feeding

and swimming. In the past, axial muscles and the vertebral column in fishes have been analyzed primarily for their role in swimming. Viewing them as feeding structures, or at least dual-function structures, offers a new framework for understanding the form-function relationships of the axial musculoskeletal system. Similarly, viewing the cranial musculoskeletal system as a power transmitter, rather than solely a power generator, may yield new insights into its evolutionary and functional morphology.

To date this suction power analysis has been published for just two species, largemouth bass and bluegill sunfish, and it remains to be determined whether axial musculature is the primary source for power in fishes with different mouth and body forms and/or distant phylogenetic relationship to these two centrarchid fishes. There are several reasons to predict that axial power is widespread: 1) in ray-finned fishes, the mass of the axial musculature greatly exceeds that of the cranial musculature; 2) cranial elevation and epaxial and hypaxial muscle activity are primitive for Actinopterygii (Lauder 1980); and 3) largemouth bass and bluegill sunfish have substantially different cranial morphologies and feeding kinematics (Higham et al. 2006), suggesting axial-powered suction feeding is not limited to a single set of morphologies or behaviors.

If, as we expect, axial power does turn out to be widespread, then we'll have a new framework for studying morphology and biomechanics of ray-finned fishes. This new framework will facilitate the study of form-function relationships throughout the entire fish body. Since the vast majority of the more than 30,000 species of ray-finned fishes feed at least partially by suction, we may be on the verge of a powerful new understanding of overall body shape, of axial form and function, and of cranial form and function in over half of all vertebrate species.

2.5 Potential Future Applications of XROMM and Fluoromicrometry to Feeding Systems

XROMM will continue to yield fundamental insights into feeding systems through the measurement of 3D motion at joints and the relation of jaw kinematics to the function of teeth during chewing. XROMM will also be key for exploring the sources of muscle power for suction

feeding in diverse species of fishes. The use of XROMM and fluoromicrometry to study tongue and cheek kinematics in mammals has just begun and shows great promise. In aquatic animals, food handling during transport and processing is generally controlled by precise water motions known as the hydrodynamic tongue. With the exception of some work on lungfish (Bemis and Lauder 1986), form-function relationships of the hydrodynamic tongue have hardly been explored at all. In general, the study of food transport and swallowing across all vertebrates are areas that XROMM and fluoromicrometry have particular potential to revolutionize in the near future.

In studies of food processing, XROMM has the potential to start to show how teeth actually interact with the food and each other. Tooth form and function have often been studied from the perspective of upper and lower teeth interacting, but of course teeth rarely interact directly because there is food between them. The effects of food bolus breakdown on jaw kinematics and tooth occlusion can be quantified with XROMM (Fig. 2.3). Food breakdown requires putting some energy (work) into the food to create more surface area. XROMM and fluoromicrometry together have the potential to link muscle work to work done on the food via 3D jaw and tooth kinematics.

Another area that would be exciting to explore with XROMM and fluoromicrometry is the form-function relationships of muscles and tendons in feeding systems. In studies of locomotion, a great deal of experimental and conceptual work has been done to develop principles of muscle-tendon function. The roles of muscles and tendons in producing force, work and power have been clearly defined, as have their roles in energy conservation, power amplification and power attenuation (reviewed in (Roberts and Azizi 2011)). The effects of fundamental muscle properties, such as length-tension and force-velocity, have been explored in many forms of locomotion (reviewed in (Biewener 2016)). Such principles of muscle and tendon function have not been so clearly defined for feeding systems, but XROMM and fluoromicrometry have the potential to provide in vivo data toward such a synthesis.

In particular integrating detailed muscle architecture data from DiceCT, in vitro muscle mechanics data and in vivo muscle and tendon length changes from XROMM and

fluoromicrometry may be a powerful combination. Similar XROMM work showed that the length-tension properties of the pharyngeal jaw levator in black carp limits both the largest and smallest mollusks shells that can be crushed (Gidmark et al. 2013). But the architecture of the levator muscle is very simple, with no tendon introducing series elastic compliance into the system. The multipennate masseter muscle of mammals offers a much more complex problem. The masseter must have one or more aponeuroses for pennate fiber attachment, and that these tendinous tissues introduce series compliance can be easily felt in one's own masseter (and temporalis): bring your teeth into occlusion and then bite gradually harder and you'll feel the muscles bulging out as their fibers shorten with no change in jaw position. The fibers can only shorten because the tendons are lengthening, and increasing force increases the fiber shortening, tendon lengthening and muscle bulging. Muscle bulging is known to feed back into force and speed of shortening through dynamic architectural changes in fiber orientation (Azizi et al. 2008; Brainerd and Azizi 2005). The complex architecture of some feeding muscles, such as the mammalian muscles of mastication and the multi-part adductor mandibulae of fishes, are ripe for exploration with DiceCT, fluoromicrometry and XROMM.

Lastly, these emerging techniques offer the opportunity to study the feeding roles of structures outside the head: the vertebral column, shoulder girdle, and neck. While feeding studies may predominantly focus on the head alone, the head and body are connected anatomically—either directly (in non-tetrapod fish) or via the neck (in tetrapods)—and likely mechanically as well. This connection can be seen most clearly ray-finned fishes where the body muscles generate power for suction feeding, and the vertebral column and pectoral girdle transmit that power to the feeding apparatus. While flexion of the vertebral column has not yet been measured during suction feeding, XROMM studies of ray-finned fishes have confirmed that the pectoral girdle swings caudally to help expand the mouth cavity (Camp and Brainerd, 2014; Camp et al., 2015; Camp et al., 2018). Pectoral girdle motion has also been found to contribute to mouth expansion in a suction-feeding shark (Camp et al., 2017), even though it lacks any skeletal articulation with the skull. These results demonstrate that, like the body muscles, the pectoral girdle can have a dual-role in feeding and locomotion, and both these roles have likely influenced its evolution and morphology. XROMM and fluoromicrometry are excellent tools for

investigating how widespread these roles are among ray-finned and cartilaginous fishes, and whether the neck may perform similar functions during feeding in tetrapods.

One final advance by researchers studying the functional morphology of feeding systems will also be critical for moving the field forward, and that is data archiving and sharing. Comparative biology depends on comparing species, but for too long we have tended to collect and store data without much thought to sharing and reuse. The functional morphology research community, and feeding researchers in particular, are leading the way toward open data sharing in organismal biology. A database for EMG studies of mammalian feeding has been established, the FEED database (Wall et al. 2011), as well as standards and databases for X-ray video and standard video management (Brainerd et al. 2017), and standards for CT data management (Davies et al. 2017). The ability to synthesize results collected from many species, combined with new in vivo and in silico methods, suggest exciting years ahead in the functional morphology of vertebrate feeding systems.

2.6 Acknowledgements

Preparation of this chapter was supported in part by the US National Science Foundation under grant number 1655756 to ALC and ELB and number 1661129 to ELB, and by the UK Biotechnology and Biosciences Research Council under a Future Leader Fellowship to ALC.

Anderson RA, McBrayer LD, Herrel A (2008) Bite force in vertebrates: opportunities and caveats for use of a nonpareil whole-animal performance measure. Biol J Linn Soc 93:709-720

Anker GC (1974) Morphology and kinetics of the head of the stickleback, *Gasterosteus aculeatus*. Trans Zool Soc London 32:311-416

Ardran G, Kemp F, Ride W (1958) A radiographic analysis of mastication and swallowing in the domestic rabbit: *Oryctolagus cuniculus* (L). J Zool 130:257-274

Astley HC, Roberts TJ (2012) Evidence for a vertebrate catapult: elastic energy storage in the plantaris tendon during frog jumping Biol Lett 8:386-389. doi:10.1098/rsbl.2011.0982

Azizi E, Brainerd EL, Roberts TJ (2008) Variable gearing in pennate muscles. P Natl Acad Sci USA 105:1745-1750

Azizi E, Roberts TJ (2009) Biaxial strain and variable stiffness in aponeuroses. J Physiol 587:4309-4318

Becht G (1953) Comparative biologic-anatomical researches on mastication in some mammals I and II. Koninkl Neder Akad van Wet Proc 56:508-527

Bemis WE, Lauder GV (1986) Morphology and function of the feeding apparatus of the lungfish, *Lepidosiren paradoxa* (Dipnoi). J Morphol 187:81-108
Berquist RM et al (2012) The Digital Fish Library: using MRI to digitize, database, and document the morphological diversity of fish. PloS One 7(4):e34499. doi.org/10.1371/journal.pone.0034499
Biewener AA (2016) Locomotion as an emergent property of muscle contractile dynamics. J Exp Biol 219:285-294. doi:10.1242/jeb.123935
Brainerd EL, Azizi E (2005) Muscle fiber angle, segment bulging and architectural gear ratio in segmented musculature. J Exp Biol 208:3249-3261
Brainerd EL, Baier DB, Gatesy SM, Hedrick TL, Metzger KA, Gilbert SL, Crisco J (2010) X-ray Reconstruction of Moving Morphology (XROMM): precision, accuracy and applications in comparative biomechanics research. J Exp Zool A 313A:262-279
Brainerd EL, Blob RW, Hedrick TL, Creamer AT, Müller UK (2017) Data Management Rubric for Video Data in Organismal Biology. Integr Comp Biol 57:33-47
Camp AL, Astley HC, Horner AM, Roberts TJ, Brainerd EL (2016) Fluoromicrometry: a method for measuring muscle length dynamics with biplanar videofluoroscopy. J Exp Zool A 325A: 399-408. doi:10.1002/jez.2031
Camp AL, Brainerd EL (2014) Role of axial muscles in powering mouth expansion during suction feeding in largemouth bass (*Microterus salmoides*). J Exp Biol 217:1333-1345. doi:10.1242/jeb.095810
Camp AL, Brainerd EL (2015) Reevaluating Musculoskeletal Linkages in Suction-Feeding Fishes with X-Ray Reconstruction of Moving Morphology (XROMM). Integr Comp Biol 55:36-47. doi:10.1093/icb/icv034
Camp AL, Roberts TJ, Brainerd EL (2015) Swimming muscles power suction feeding in largemouth bass Proc Natl Acad Sci U S A 112:8690-8695 doi:10.1073/pnas.1508055112
Camp AL, Scott B, Brainerd EL, Wilga CD (2017) Dual function of the pectoral girdle for feeding and locomotion in white-spotted bamboo sharks Proc Biol Sci 284 doi:10.1098/rspb.2017.0847
Camp AL, Roberts TJ, Brainerd EL (2018) Bluegill sunfish use high power outputs from axial muscles to generate powerful suction-feeding strikes J Exp Biol 221: jeb178160 doi: 10.1242/jeb.178160
Carroll AM (2004) Muscle activation and strain during suction feeding in the largemouth bass *Micropterus salmoides*. J Exp Biol 207:983-991. doi:10.1242/jeb.00862
Carroll AM, Wainwright PC (2006) Muscle function and power output during suction feeding in largemouth bass, *Micropterus salmoides*. Comp Biochem Physiol A Mol Integr Physiol 143:389-399. doi:10.1016/j.cbpa.2005.12.022
Conroy GC, Vannier MW (1984) Noninvasive three-dimensional computer imaging of matrix-filled fossil skulls by high-resolution computed tomography. Science 226:456-458
Cranford TW (1988) The anatomy of acoustic structures in the spinner dolphin forehead as shown by X-ray computed tomography and computer graphics. In Nachtigall P.E., Moore P.W.B. (eds) Animal Sonar. NATO ASI Science (Series A: Life Sciences), vol 156. Springer, Boston, pp 67-77
Davies TG et al. (2017) Open data and digital morphology. Proc Biol Sci 284 doi:10.1098/rspb.2017.0194
Davis JS (2014) Functional morphology of mastication in musteloid carnivorans. Ph.D. Dissertation, Ohio University

Dawson MM, Metzger KA, Baier DB, Brainerd EL (2011) Kinematics of the quadrate bone during feeding in Mallard ducks. J Exp Biol 214:2036-2046

Drost, M. R., Vandenboogaart, J. G. M., 1986. A simple method for measuring the changing volume of small biological objects, illustrated by studies of suction feeding by fish larvae and of shrinkage due to histological fixation. J Zool 209:239-249.

Gans C, Vree Fd, Gorniak GC (1978) Analysis of mammalian masticatory mechanisms: progress and problems. Anat Histol Embryol 7:226-244

Gatesy SM, Baier DB, Jenkins FA, Dial KP (2010) Scientific Rotoscoping: a morphology-based method of 3-D motion analysis and visualization. J Exp Zool 313A:244-261

Gibb AC, Ferry-Graham L (2005) Cranial movements during suction feeding in teleost fishes: Are they modified to enhance suction production? Zoology (Jena) 108:141-153. doi:10.1016/j.zool.2005.03.004

Gidmark NJ, Staab KL, Brainderd EL, Hernandez LP (2012). Flexibility in starting posture drives flexibility in kinematic behvior of the kinethmoid-mediated premaxillary protrusion mechanism in a cyprinid fish, *Cyprinus carpio*. J Exp Biol 215:2262-2272.

Gidmark NJ, Konow N, LoPresti E, Brainerd EL (2013) Bite force is limited by the force–length relationship of skeletal muscle in black carp, *Mylopharyngodon piceus*. Biol Lett 9:20121181

Gidmark NJ, Tarrant JC, Brainerd EL (2014) Convergence in morphology and masticatory function between the pharyngeal jaws of grass carp, *Ctenopharyngodon idella*, and oral jaws of amniote herbivores. J Exp Biol 217:1925-1932

Gignac PM, Kley NJ (2014) Iodine-enhanced micro-CT imaging: Methodological refinements for the study of the soft-tissue anatomy of post-embryonic vertebrates. J Exp Zool B 322:166-176

Gignac PM et al. (2016) Diffusible iodine-based contrast-enhanced computed tomography (diceCT): an emerging tool for rapid, high-resolution, 3-D imaging of metazoan soft tissues. J Anat 228:889-909

Gold MEL, Schulz D, Budassi M, Gignac PM, Vaska P, Norell MA (2016) Flying starlings, PET and the evolution of volant dinosaurs. Curr Biol 26:R265-R267

Grobecker DB, Pietsch TW (1979) High-speed cinematographic evidence for ultrafast feeding in antennariid anglerfishes. Science 205:1161

Gröning F, Jones ME, Curtis N, Herrel A, O'Higgins P, Evans SE, Fagan MJ (2013) The importance of accurate muscle modelling for biomechanical analyses: a case study with a lizard skull. J Roy Soc Interface 10:20130216

Grosse IR, Dumont ER, Coletta C, Tolleson A (2007) Techniques for modeling muscle-induced forces in finite element models of skeletal structures. Anat Rec (Hoboken) 290:1069-1088. doi:10.1002/ar.20568

Grossnickle DM (2017) The evolutionary origin of jaw yaw in mammals. Sci Rep 7:45094

Herrel A, De Grauw E, Lemos-Espinal JA (2001) Head shape and bite performance in xenosaurid lizards. J Exp Zool A 290:101-107

Higham TE, Day SW, Wainwright PC (2006) Multidimensional analysis of suction feeding performance in fishes: fluid speed, acceleration, strike accuracy and the ingested volume of water. J Exp Biol 209:2713-2725. doi:10.1242/jeb.02315

Hylander WL (1977) In vivo bone strain in the mandible of *Galago crassicaudatus.* Am J Phys Anthropol 46:309-326

Iriarte-Diaz J, Terhune CE, Taylor AB, Ross CF (2017) Functional correlates of the position of the axis of rotation of the mandible during chewing in non-human primates. Zoology 124:106-118

Jeffery NS, Stephenson RS, Gallagher JA, Jarvis JC, Cox PG (2011) Micro-computed tomography with iodine staining resolves the arrangement of muscle fibres. J Biomech 44:189-192

Knörlein BJ, Baier DB, Gatesy SM, Laurence-Chasen JD, Brainerd EL (2016) Validation of XMALab Software for Marker-based XROMM. J Exp Biol 219:3701-3711. doi:10.1242/jeb.145383

Konow N, Cheney JA, Roberts TJ, Waldman JR, Swartz SM (2015) Spring or string: does tendon elastic action influence wing muscle mechanics in bat flight? Proc Biol Sci 282:20151832 doi:10.1098/rspb.2015.1832

Konow N, Thexton A, Crompton A, German RZ (2010) Regional differences in length change and electromyographic heterogeneity in sternohyoid muscle during infant mammalian swallowing. J App Physiol 109:439-448

Lauder GV (1980) Evolution of the feeding mechanism in primitive actinopterygian fishes: a functional anatomical analysis of *Polypterus*, *Lepisosteus*, and *Amia*. J Morphol 163:283-317

Lauder GV, Madden PG (2008) Advances in comparative physiology from high-speed imaging of animal and fluid motion. Annu Rev Physiol 70:143-163

Liem KF (1967) Functional morphology of the head of the anabantoid teleost fish, *Helostoma temmincki.* J Morphol 121:135-157

Liem KF (1980) Acquisition of energy by teleosts: adaptive mechanisms and evolutionary patterns. In: Ali M.A. (eds) Environmental Physiology of Fishes. NATO Advanced Study Institutes Series (Series A: Life Science), vol 35. Springer, Boston, pp 299-334

MacCannell A, Sinclair K, Friesen-Waldner L, McKenzie CA, Staples JF (2017) Water–fat MRI in a hibernator reveals seasonal growth of white and brown adipose tissue without cold exposure. J Comp Physiol B 187:759-767

Menegaz RA, Baier DB, Metzger KA, Herring SW, Brainerd EL (2015) XROMM analysis of tooth occlusion and temporomandibular joint kinematics during feeding in juvenile miniature pigs. J Exp Biol 218:2573-2584. doi:10.1242/jeb.119438

Metscher BD (2009) MicroCT for comparative morphology: simple staining methods allow high-contrast 3D imaging of diverse non-mineralized animal tissues. BMC Physiol 9:11

Montie EW, Schneider GE, Ketten DR, Marino L, Touhey KE, Hahn ME (2007) Neuroanatomy of the subadult and fetal brain of the Atlantic White-sided Dolphin (*Lagenorhynchus acutus*) from in situ magnetic resonance images. Anat Rec 290:1459-1479

Montuelle SJ, Williams SH (2015) In vivo measurement of mesokinesis in *Gekko gecko*: the role of cranial kinesis during gape display, feeding and biting. PloS One 10:e0134710 doi:10.1371/journal.pone.0134710

Moyers RE (1950) An electromyographic analysis of certain muscles involved in temporomandibular movement. Amer J Orthodontics 36:481-515

Muller M, Osse J (1984) Hydrodynamics of suction feeding in fish. Trans Zool Soc London 37:51-135

Muller M, Osse J, Verhagen J (1982) A quantitative hydrodynamical model of suction feeding in fish. J Theor Biol 95:49-79

Olsen AM, Camp AL, Brainerd EL (2017) The opercular mouth-opening mechanism of largemouth bass functions as a 3D four-bar linkage with three degrees of freedom. J Exp Biol 220:4612-4623
Olsen AM, Hernandez LP, Camp AL, Brainerd EL (2017) Linking morphology and motion: Testing multibody simulations against in vivo cranial kinematics in suction feeding fishes using XROMM. The FASEB Journal 31:90.91-90.91
Olsen AM, Westneat MW (2016) Linkage mechanisms in the vertebrate skull: Structure and function of three-dimensional, parallel transmission systems. J Morphol 277:1570-1583
Orsbon CP, Gidmark NJ, Ross CF (2017) Analysis of the Primate "Squeeze-back" Swallowing Mechanism using X-ray Reconstruction of Moving Morphology and Fluoromicrometry. The FASEB Journal 31:393.391-393.391
Orsbon, CP, Gidmark, NJ, Ross, CF (2018) Dynamic Musculoskeletal Functional Morphology: Integrating diceCT and XROMM. Anat. Rec. 301, 378–406.
Osse JWM (1969) Functional morphology of the head of a perch (*Perca fluviatilis* L.): An electromyographic study. Neth J Zool 19:289-392
Oufiero CE, Holzman RA, Young FA, Wainwright PC (2012) New insights from serranid fishes on the role of trade-offs in suction-feeding diversification. J Exp Biol 215:3845-3855 doi:10.1242/jeb.074849
Phelps ME (2000) Positron emission tomography provides molecular imaging of biological processes. P Nat Acad Sci USA 97:9226-9233
Rayfield EJ (2007) Finite Element Analysis and Understanding the Biomechanics and Evolution of Living and Fossil Organisms. Annu Rev Earth Pl Sc 35:541-576. doi:10.1146/annurev.earth.35.031306.140104
Roberts TJ, Azizi E (2011) Flexible mechanisms: the diverse roles of biological springs in vertebrate movement. J Exp Biol 214:353-361
Rowe T, Brochu CA, Kishi K (1999) Cranial morphology of *Alligator mississippiensis* and phylogeny of Alligatoroidea. Northbrook, III, Society of Vertebrate Paleontology Memoir 6. Journal of Vertebrate Paleontology 19 (supplement to 2):1-100
Rowe T, Carlson W, Bottorff W (1995) Thrinaxodon: digital atlas of the skull CD-ROM (Second Edition, for Windows and Macintosh platforms) University of Texas Press, Austin, Texas 547
Sanford CP, Wainwright PC (2002) Use of sonomicrometry demonstrates the link between prey capture kinematics and suction pressure in largemouth bass. J Exp Biol 205:3445-3457
Van Wassenbergh S, Aerts P (2009) Aquatic suction feeding dynamics: insights from computational modelling. J R Soc Interface 6:149-158 doi:10.1098/rsif.2008.0311
Van Wassenbergh S, Aerts P, Herrel A (2005a) Scaling of suction-feeding kinematics and dynamics in the African catfish, *Clarias gariepinus*. J Exp Biol 208:2103-2114
Van Wassenbergh S, Herrel A, Adriaens D, Aerts P (2005b) A test of mouth-opening and hyoid-depression mechanisms during prey capture in a catfish using high-speed cineradiography. J Exp Biol 208:4627-4639 doi:10.1242/jeb.01919
Van Wassenbergh S, Strother JA, Flammang BE, Ferry-Graham LA, Aerts P (2008) Extremely fast prey capture in pipefish is powered by elastic recoil. J R Soc Interface 5:285-296 doi:10.1098/rsif.2007.1124
Wall CE, Vinyard CJ, Williams SH, Gapeyev V, Liu X, Lapp H, German RZ (2011) Overview of FEED, the feeding experiments end-user database. Integr Comp Biol 51:215-223

Watson PJ, Groning F, Curtis N, Fitton LC, Herrel A, McCormack SW, Fagan MJ (2014) Masticatory biomechanics in the rabbit: a multi-body dynamics analysis. J R Soc Interface 11 doi:10.1098/rsif.2014.0564

Weijs W, De Jongh H (1977) Strain in mandibular alveolar bone during mastication in the rabbit. Arch Oral Biol 22:667-675

Westneat MW (1990) Feeding mechanics of teleost fishes (Labridae; Perciformes): A test of four-bar linkage models. J Morphol 205:269-295 doi:10.1002/jmor.1052050304

Westneat MW (1994) Transmission of force and velocity in the feeding mechanisms of labrid fishes (Teleostei: Perciformes). Zoomorphology 114:103-118 doi:10.1007/bf00396643

Figure Legends

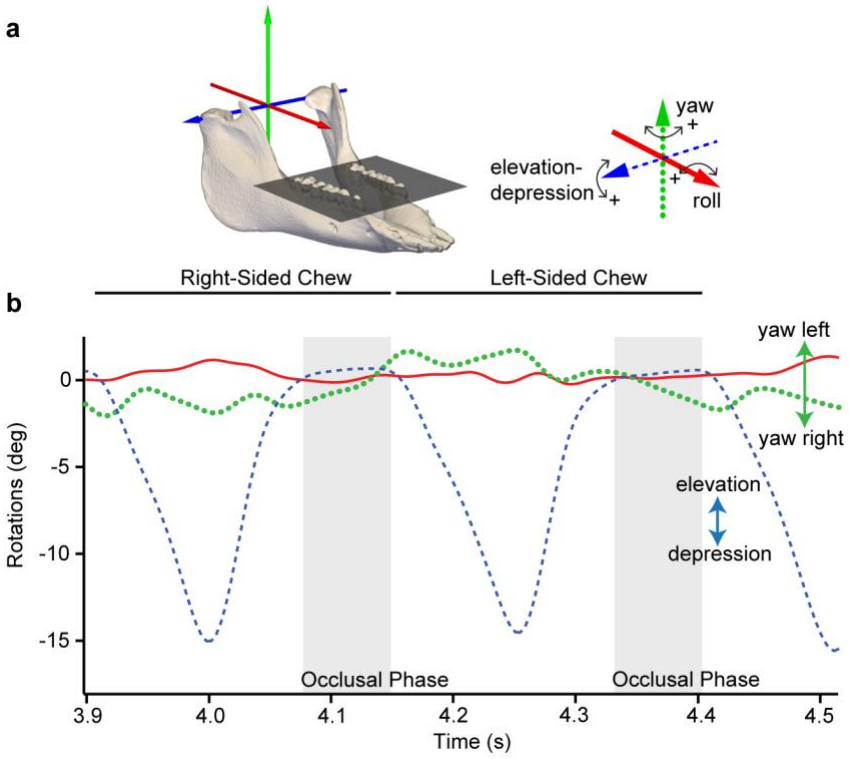

Fig. 2.1 Yaw of the mandible in alternating left-right chewing cycles in a miniature pig. **a** Joint coordinate system used to measure motion of the mandible relative to the cranium (not shown) as rotation about a dorsoventral axis (yaw, *green dotted axis*), a mediolateral axis (depression and elevation, *blue dashed axis*), and a rostrocaudal axis (roll, *red solid axis*). **b** Mandibular rotation about each axis (colors as in panel **a**) during chewing cycles, along with the occlusal phase (*grey bars*). (Modified from Menegaz et al., 2015)

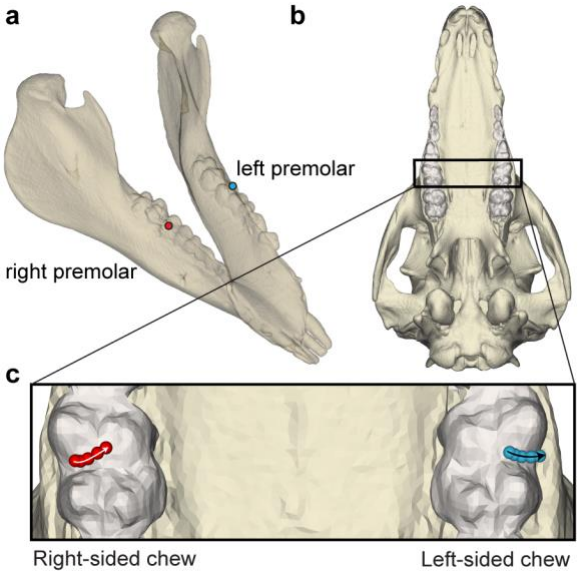

Fig. 2.2 Oblique stroke of lower premolars against upper premolars during occlusion in a miniature pig. **a** Spheres were fitted to the cusp of a left (*blue*) and right (*red*) lower premolar to trace their motion as part of the XROMM-animated mandible model. **b** Ventral view of the cranium, showing the positions of the corresponding upper premolars. **c** Ventral view of the cranium showing path of the lower premolars as superimposed spheres, with black arrows indicating the direction of the stroke during occlusion (Modified from Menegaz et al., 2015)

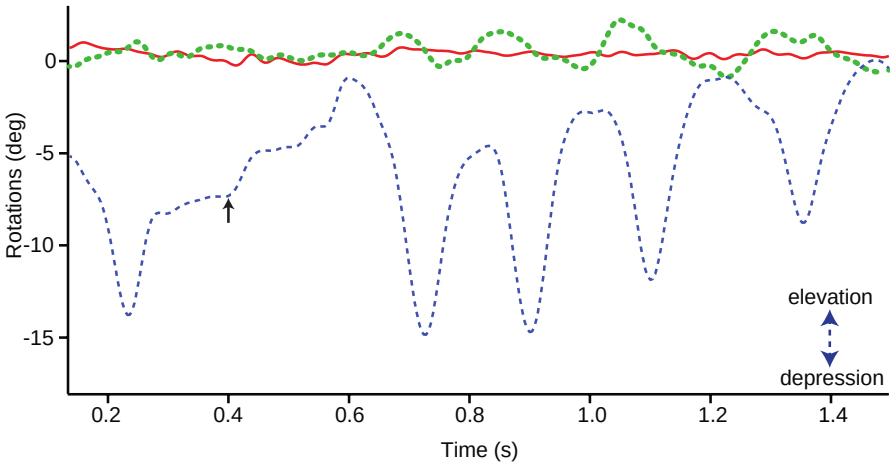

Fig. 2.3 Rotations of the mandible during breaking and reduction of nut and shell pieces in a miniature pig. Mandible rotation, relative to the cranium, was measured about a dorsoventral axis (yaw, *green dotted line*), a mediolateral axis (depression and elevation, *blue dashed line*), and a rostrocaudal axis (roll, *red solid line*) (see Fig. 2.1). Zero elevation of the mandible indicates zero gape (teeth in occlusion), and the mandible can be seen to elevate more and more toward occlusion with each chewing cycle. The time of the nut breaking is indicated by the *black arrow* (Modified from Menegaz et al., 2015.)

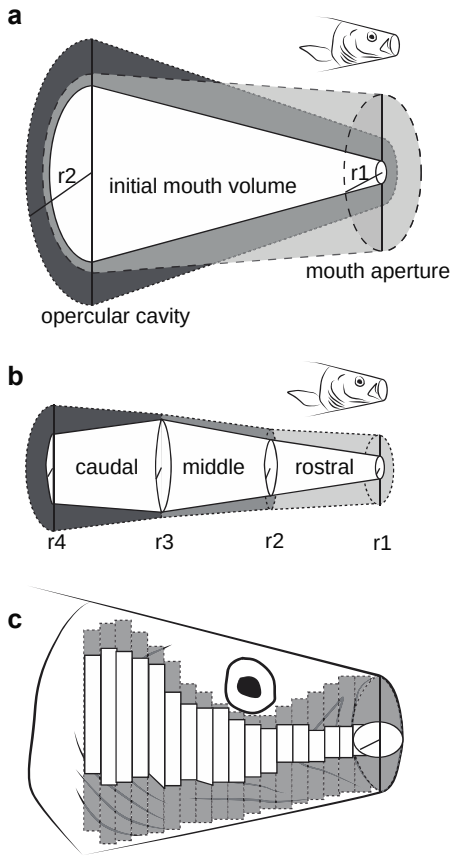

Fig. 2.4 Methods for measuring mouth volume changes from during suction feeding in fishes. **a** Volume change of the mouth cavity was initially modelled as a single expanding cone, with two radii representing the change in the mouth aperture (*r1*) and opercular cavity (*r2*) during suction feeding. The cone is shown at its initial position prior to the strike (*solid lines, white region*), at the maximum expansion of the mouth aperture (*dashed lines, light grey region*), and at the maximum expansion of the opercular cavity (*dashed lines, dark grey region*) (after Muller and Osse, 1984). **b** A modified model consisting of three truncated cones, with four radii (*r1-r4*) to allow different rostrocaudal regions of the mouth to expand at different times and rates, as is observed in live fish (after from Van Wassenbergh et al., 2006). **c** The ellipse method (Drost and Vandenboogaart, 1986) is used to calculate static mouth volume, by representing the mouth cavity as a series of ellipses and summing the volumes of each to calculate total mouth volume, for example, before the strike (*solid lines, white region*) and at peak mouth expansion (*dashed lines, grey region*). It can also be used to model mouth volume changes by dynamically changing the major and minor axes of each ellipse based on the kinematics of mouth expansion. (after Van Wassebergh et al., 2007)

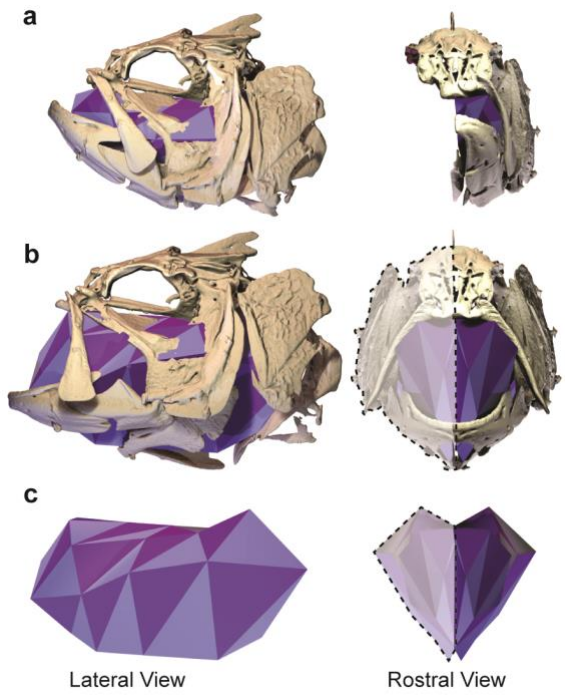

Fig. 2.5 Digital dynamic endocast for measuring mouth volume during suction feeding in largemouth bass. **a** The endocast (*purple polygon*) is fit to XROMM-animated models of the bones defining the left-side of the mouth cavity, shown here prior to suction expansion. **b** As the bones move during suction expansion, the endocast deforms and expands to fill the growing mouth cavity. The endocast and skeleton are shown here at peak expansion. **c** The volume of the endocast, shown here without the skeletal models, can be measured at every time point and doubled to calculate total mouth volume by assuming bilateral symmetry. (Modified from Camp et al., 2015)

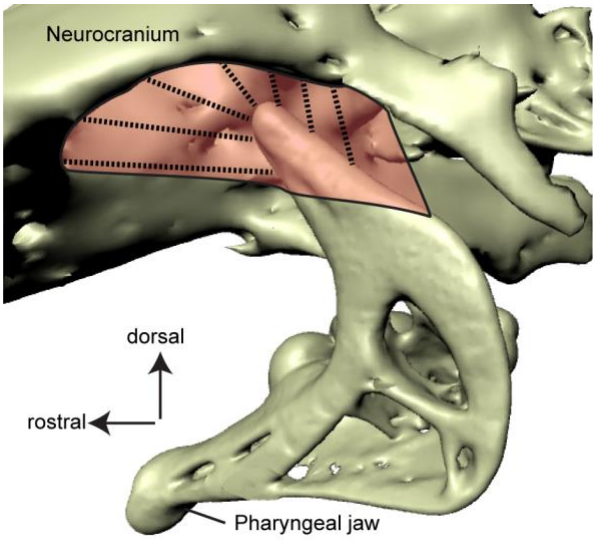

Fig. 2.6 Pharyngeal levator muscle in the black carp. The fan-shaped muscle (fibers in *dashed lines*) attaches directly to the dorsal process of the pharyngeal jaw and to the interior of the large levator fossa in the neurocranium, without tendons that would introduce series-elastic compliance. (Modified from Gidmark et al., 2013)

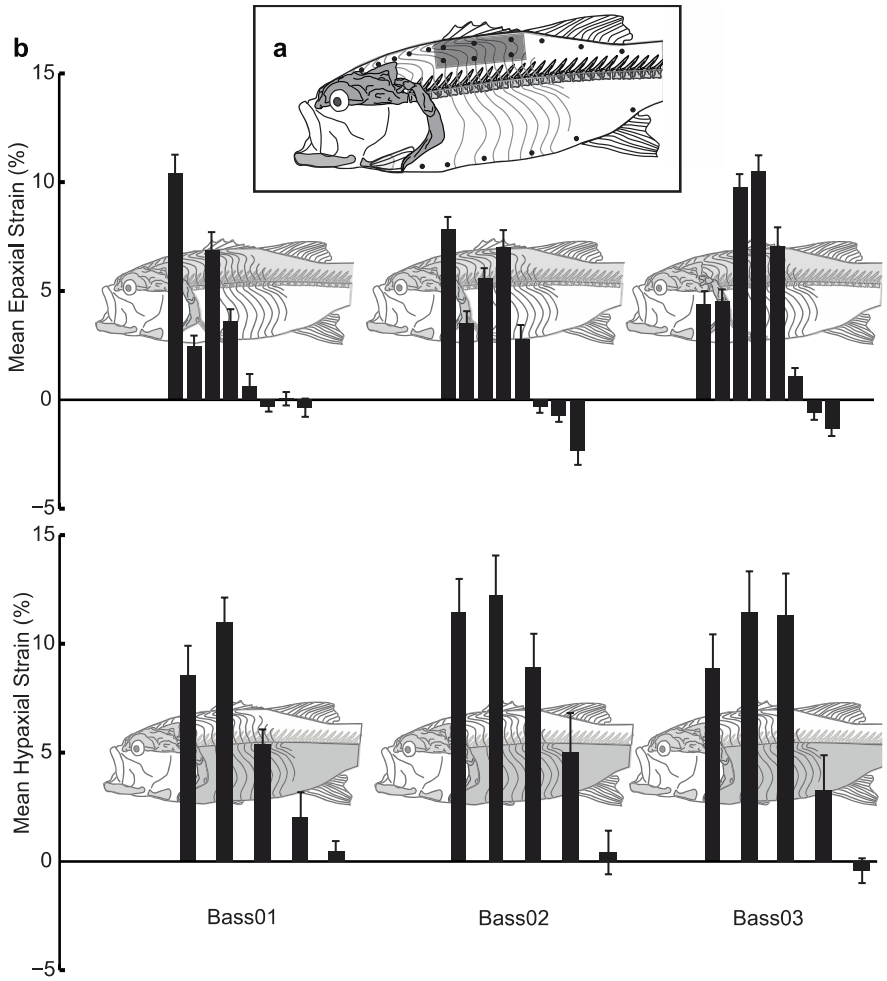

Fig. 2.7 Fluoromicrometry marker placement and muscle strain distribution during suction feeding in largemouth bass. **a** Placement of radio-opaque beads (*black circles)* used in fluoromicrometry to measure length changes along the epaxial (dorsal) and hypaxial (ventral) muscles. Six beads are also used to define a body-reference plane (*grey rectangle*) that can be used to measure cranial movements relative to the body. **b** Mean (± s.e.m.) muscle strain at peak neurocranium elevation in each region of the epaxials, and at peak pectoral girdle retraction in each region of the hypaxials for three fish (N = 10 strikes for each fish). Positive strain values indicate muscle shortening. The x-axis position of each bar represents the approximate rostrocaudal position of that muscle region. (Modified from Camp and Brainerd, 2014)

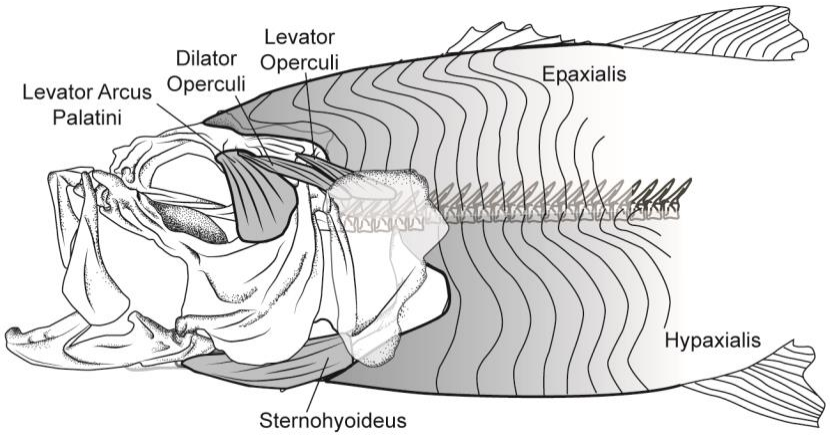

Fig. 2.8. Cranial and axial musculature in largemouth bass. The four muscles of the head (dilator operculi, levator operculi, levator arcus palatine, sternohyoideus) that can contribute to suction expansion are much smaller than the two massive axial muscles (epaxialis, hypaxialis) that can also contribute to mouth expansion during suction feeding. (Modified from Camp et al., 2015)

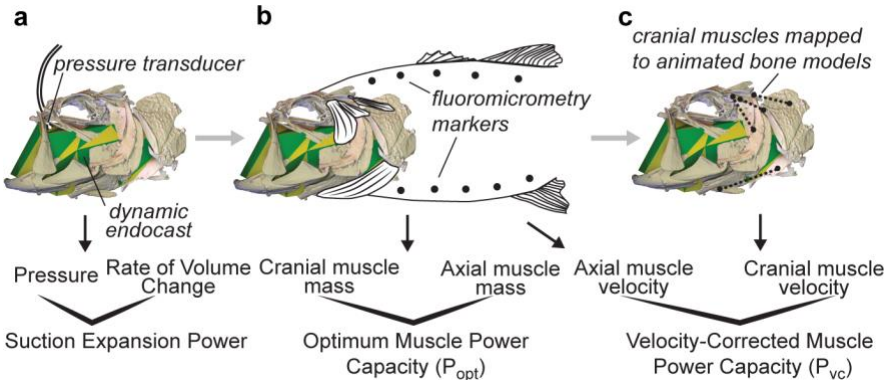

Fig. 2.9 Methods for calculating the mechanical power required for mouth expansion during suction feeding and estimating the power the cranial and axial muscles are capable of contributing to that suction expansion. **a** Instantaneous buccal pressure is estimated from a pressure transducer, then multiplied by the rate of volume change to yield instantaneous suction power. **b** Fluoromicrometry is used to measure axial muscle shortening and the extent of shortening along the body, which in turn determined the mass of axial musculature that contributes to suction feeding. **c** Cranial muscle shortening is measured from muscle fascicle attachment points mapped onto the animated cranial bones. Optimum (i.e., assuming all contractile properties are optimized to maximize power production) muscle power capacity (P_{opt}) and velocity-corrected muscle power capacity (P_{vc}) are calculated from muscle mass and measured shortening velocities, respectively.

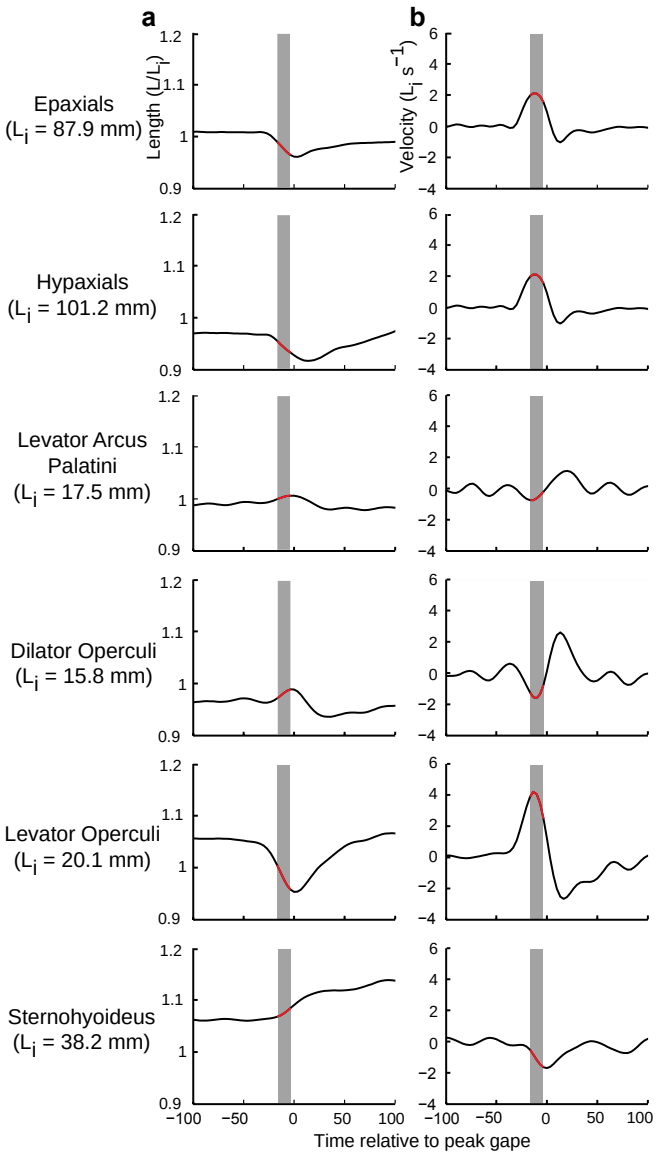

Fig. 2.10 Muscle length (**a**) and velocity (**b**) from a sample strike**.** Muscle length is shown normalized to the mean initial muscle length (L_i). Decreasing length values indicate muscle shortening. The gray bars mark the time and red regions mark the length values during which expansion power was within 25% of its maximum. Zero time is peak gape. (From Camp et al., 2015)

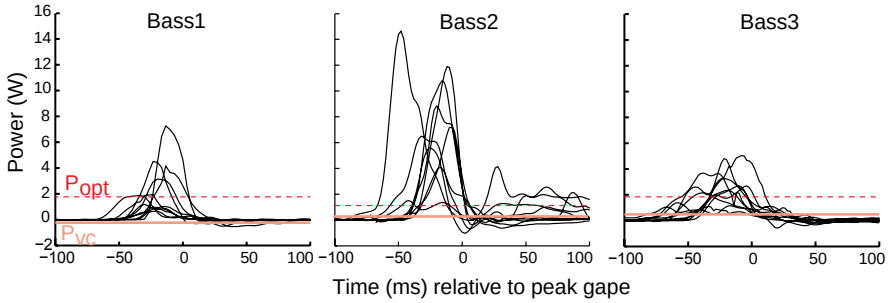

Fig. 2.11 Comparison of suction expansion power and cranial muscle power capacity for three individual largemouth bass. Mouth expansion power of all strikes (*black lines*) are graphed as a function of time for each individual. The optimum power capacity (P_{opt}, *red dashed line*) and median of the velocity-corrected power capacity (P_{vc}, *pink solid line*) of all of the cranial muscles summed together are shown for each individual. (From Camp et al., 2015)

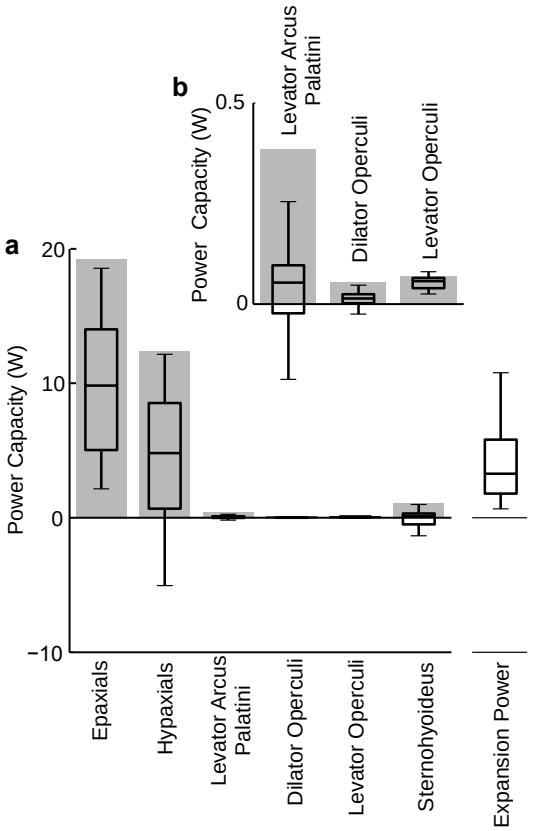

Fig. 2.12 Optimal (P_{opt}) and velocity-corrected (P_{vc}) muscle power capacities of largemouth bass. **a** For all three individuals (*n* = 29 strikes), *grey bars* show P_{opt} and *unfilled boxplots* show P_{vc}. The power required for buccal expansion is shown in a boxplot on the extreme right, and all boxplots represent the 25th and 75th percentiles of the date (*bottom and borders*), the median (*black line)* and1.5 times the interquartile range (*whiskers*). b The inset shows the same data, but with the y-axis limited to 0.5 Watts to visualize the power capacities of the smallest three cranial muscles (Modified from Camp et al., 2015)